IMPROVING DESIGN AND OPERATING PARAMETERS OF THE RECUPERATOR FOR WASTE HEAT RECOVERY FROM ROTARY KILNS

by

***Nenad P. STOJIĆ*[a], *Rade M. KARAMARKOVIĆ*[*a], *Miodrag V. KARAMARKOVIĆ*[b], *and Miloš V. NIKOLIĆ*[a]**

[a] Faculty of Mechanical and Civil Engineering in Kraljevo, University of Kragujevac, Kragujevac, Serbia
[b] Siemens AG Austria, Power and Gas, Vienna, Austria

Original scientific paper
https://doi.org/10.2298/TSCI210410239S

Depending on their applications, heat losses from the shells of rotary kilns account for 3-25% of the total heat input. Over the hottest zone of the kiln shell, an annular duct with a variable diameter is formed. Two air streams entering the annulus at both ends flow to a common extraction point to receive the thermal power equal to the ambient heat loss of the bare kiln. The design does not require airtightness, utilizes the entire heat loss, and by the variation of the air-flow can be used over the kilns with variable operating parameters (±20% heat loss), which show similar surface temperature patterns. The main disadvantage of the design is the approaching of the surfaces of the kiln and the recuperator at the outlet of preheated air. This means that for a given heat loss and a surface temperature pattern, the rotational eccentricity of the kiln shell is the most influencing parameter that defines the air preheating temperature and the efficiency of the recuperator. To solve the problem, four redesigns with: double annuluses, the usage of radiation fins, air addition, and a combination of two basic designs are analyzed by the use of analytical and CFD models. From the listed redesigns: first could be used only to prevent overheating, second has a modest positive effect, third should be applied in combination with fourth.

Key words*: recuperator, design, model, CFD, rotary kiln, energy efficiency, heat transfer, heat exchanger*

Introduction

Rotary kilns are pyroprocessing devices used to raise materials to a high temperature in a continuous process [1]. The kilns are widely applied in various technological processes such as [2]: cement production, calcination, incineration, aluminum production, activated carbon manufacturing, pyrolysis, food production*, etc.* The fact that the world cement and clinker production has increased more than 240% during the first 20 years of the 21st century [3, 4], testifies the importance of these devices. In high temperature applications of rotary kilns, heat loss from the shell to the environment plays an important role. In the cement industry, it accounts for 8-15% [5], in dead burning of magnesite 24.8% [6], in the calcination of dolomite 17.17% [1], of the total heat input. The heat loss is not uniform along with rotary kilns and depends on their application, *i.e.*, the processes that take place inside, the thermal resistance and condition of

* Corresponding author, e-mail: karamarkovic.r@mfkv.kg.ac.rs

coating and refractory layers inside them, and to a lesser extent on the environmental conditions. The problem of coating and its assessment is addressed in [7]. Several sections differ on a rotary kiln depending on temperature distribution and technological process. The best option from the standpoint of the Second law of thermodynamics is to insulate the kiln and minimize the heat loss. In some of the aforementioned applications, high temperature processes can cause overheating and endanger kiln shells. Because of that, the authors in [8, 9], planned observation windows on the secondary insulating shell, whereas other authors have managed to use the loss for:

– Electricity generation as an array of thermoelectric generation (TEG) units arranged on a secondary shell coaxial with a rotary kiln [10, 11]. The temperature gradient between the two ends of the TEG modules results in the generation of electricity as a result of the Seebeck effect. The layer of TEG modules also acts as thermal insulation, because thermo-electric materials usually have low thermal conductivity [10].
– Water heating. Caputo *et al.* [5], developed and optimized the design of a recuperator for water heating that utilizes the radiant heat loss from the shell of a rotary kiln. The utilized heat is used in a district heating system. Another water heater, which is used as a heat source for absorption water chiller is presented in [12]. It also uses only the radiant component of the heat loss. Through experimental investigations and numerical simulations, Du *et al*. [13] and Yin *et al.* [14, 15], presented and optimized a water heater that uses heat loss from a rotary kiln in a cement factory. In [13], the authors experimentally investigated three different variants of the developed exchanger, which consists of a radiant type exchanger in a hexagonal shell that uses radiant heat loss and one or two layers of coiled pipes that use convective component of the heat loss. In the design, air-flows vertically between the kiln and the exchanger due to the diameter of 4060 mm.

In contrast to the presented systems, a recuperator that uses heat loss from the shell of a rotary kiln for combustion air preheating was presented in [1]. Above the hottest zone of the kiln, where the highest temperatures of the shell are located, an annular duct with a variable diameter is formed. Two air streams entering the annulus at both ends flow to a common extraction point by the use of a fan. The annulus is dimensioned so that the air receives a heat flow rate equal to the heat loss from the bear kiln, fig. 1(a) illustrates the solution. The design does not require airtightness and utilizes the entire heat loss: radiant and convective.

Figure 1(b) shows the side view from the recuperator drawing. The design consists of two symmetrical covers – 1 that move on the horizontal rails – 2. A constant force of the hydraulic cylinders – 3 connects the covers – 1. In the case of a need or urgency, unloading of the hydraulic cylinders – 3 separates the covers – 1. The weights – 4 detach the recuperator. The inner of the covers – 1 are semicylindrical metal surfaces – 5 with a predetermined radius that touch each other in two lines of contact – 6. Two rows of screws – 7 regulate the airtightness and the distance between the semicylindrical surfaces – 5. The assembly of the covers – 1 and the kiln – 8 forms an annular gap for air-flow. The contact lines of the semicylindrical surfaces – 5 are filled with a sealing material. Mineral wool protected with an aluminum sheet – 9 prevents heat loss from the surfaces – 5. The fan – 10 extracts air-flow over the hottest zone of the kiln by the use of two flexible ducts – 11. The recuperator uses radial blinds at both ends to control air-flows. A modification of the presented principle with an extra annulus filled with a phase-change material was experimentally investigated in [16].

The design shown in fig. 1 is simple, cost-effective, uses the entire heat loss, prevents overheating, and does not influence the technological process within the kiln. Nevertheless, some conditions disfavor its usage. Because of its compressibility, the air is not an economical heat carrier at distances longer than a few tens of meters. However, the main disadvantage of

the design is the approach of the kiln and recuperator surfaces at the outlet of preheated air, see fig. 1(a). This happens at the air exit from the annulus, where the temperature difference between the air and the kiln is the smallest. The air needs higher heat transfer coefficients and therefore, higher velocities to receive the precise amount of heat with a given surface area. This could be an insurmountable problem for the kilns with large rotational eccentricities. Zheng *et al*. [17], demonstrates the significance of the problem, and in that respect, the position of the recuperator relative to the supporting roller bearing is important.

Regarding the defined problem, the goals of the paper are:

– to analyze the performance of the recuperator shown in fig. 1 depending on the rotational eccentricity, to examine its behavior in an unsteady operation, and to find the design parameters that will increase the distance between the kiln and the recuperator and
– to present and analyze redesigns so as the air is preheated to the highest possible temperature.

The simplest way to solve the defined problem is to increase the air-flow. However, this approach decreases the exergy efficiency of the recuperator because of a lower preheating temperature and requires finding the use of preheated air other than for combustion. One way to find the optimal usage of preheated air is to employ the pinch analysis as in [18].

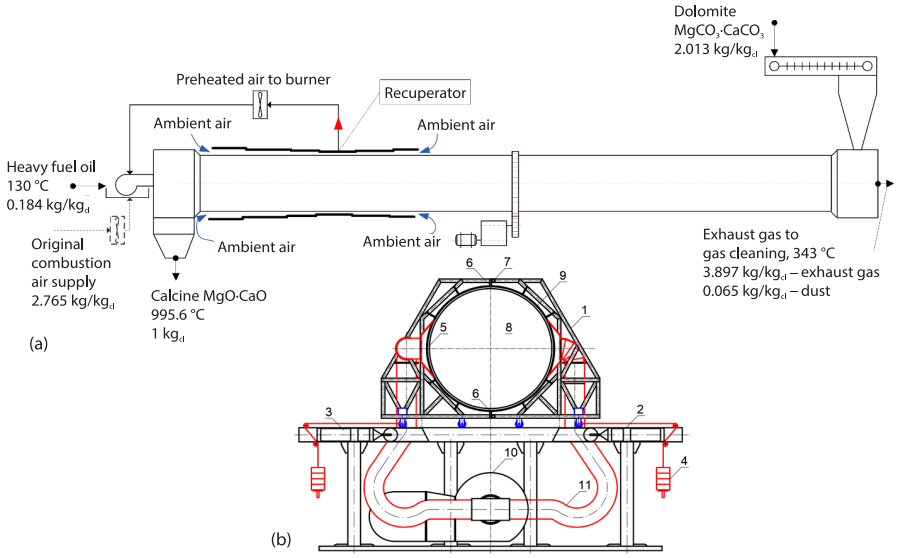

Figure 1. (a) The concept of the annular recuperator together with the mass balance of the examined kiln and (b) side drawing of the recuperator [1]

Proposed redesigns and improved operating parameters

Figure 2 shows three redesigns used to achieve the second goal. Figure 2(a) depicts the recuperator with parallel passages (RPP). The RPP intends to:

– decrease air velocity in the inner annulus and consequently increase the distance between the kiln and the recuperator and
– promote heat transfer to the air in the outer annulus, which does not have the problem of eccentricity and can be narrowed and finned.

In the inner passage, the air should be heated by the convective, and in the outer passage by the radiative heat loss. From a thermodynamic perspective, the most preferable option would be the isothermal mixing of all four air streams at the exit.

Figure 2(b) depicts the recuperator with an additional perforated cylindrical surface, which is a sort of radiation fins (RF). Their role is to:

– receive a part of the radiation from the kiln surface and by an additional surface area to transfer it to the air and to enable an optimal part of the heat radiation from the kiln surface to reach the recuperator.

The solution enlarges the heat transfer area in the recuperator and hence decreases the air velocity in the annulus. The decreased velocity consequently leads to an increase in the critical distance. The perforated RF should be connected to the recuperator. The RF could also be connected to the kiln, but the intention is to use the unavoidable heat loss and not to extract the heat from the kiln.

Figure 2(c) depicts the recuperator that uses an additional air-flow in the critical sections (RAA). The additional air-flow is introduced in front of the air outlet section, which has the smallest diameter. As a result, the critical distance would increase. The additional flow is easily controllable and does not require extra electricity consumption. To achieve the isothermal mixing, which is the most preferable option, a combination of two recuperators, as in fig. 2(d) would be preferable. The air addition before the critical section could be used in the basic solution, see fig. 1, as a backup to prevent overheating. This is the simplest way to enlarge the critical distance. Apart from its usage for combustion, the sensible heat of air could be utilized

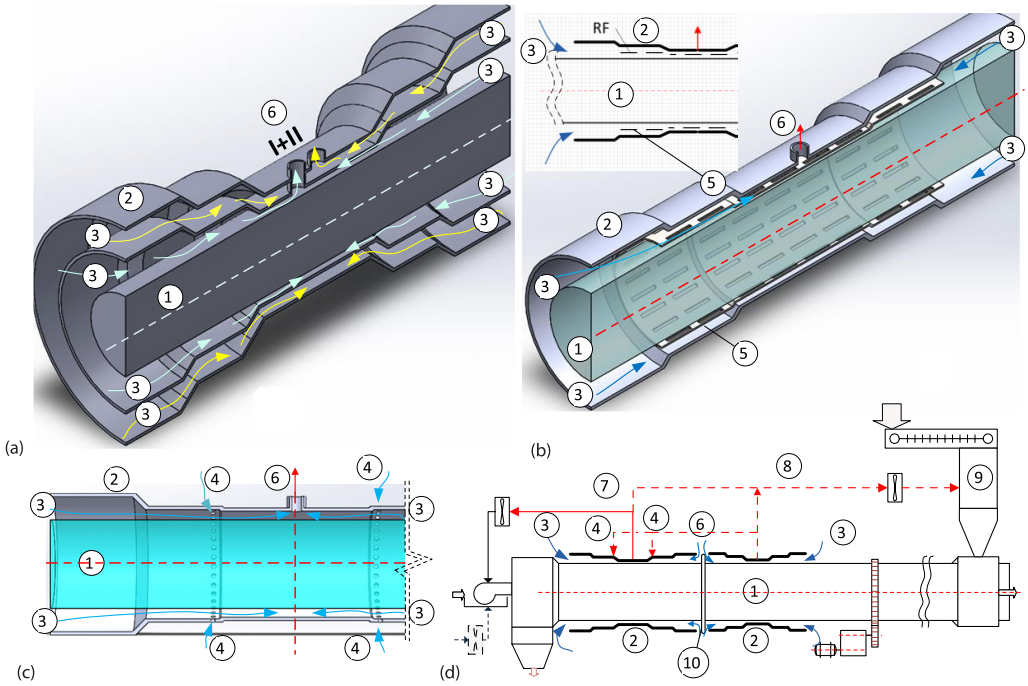

Figure 2. The analyzed redesigns of the recuperator; (a) with parallel passages (RPP), (b) with an additional cylindrical perforated surface (RF), (c) with the introduction of additional air (RAA), and (d) two recuperators and the potential usage of preheated air for combustion and feed preheating (dashed lines represent optional solutions); *1 – rotary kiln, 2 – recuperator, 3 – air-flow, 4 – additional air, 5 – cylindrical fins, 6 – exit of the preheated air, 7 – combustion air, 8 – air used to preheat the feed, 9 – heat recovery to solids, and 10 – rotary kiln tyre ring*

to preheat the feed by the direct contact with dolomite, as it is shown in fig. 2(d). This solution could be applied to rotary kilns that have tyres over their hottest zones.

Behind the defined goals, the motive for the paper was the implementation of the basic solution on rotary kilns with large rotational eccentricities, varying operating conditions, and tyres over their warmest zones. These redesigns have not been implemented in practice, and their implementation by the use of cell and CFD modelling methods is analyzed in the paper.

Case study of the heat loss from the shell of a rotary kiln

Figure 1 schematically shows the mass balance of a rotary kiln, over which the recuperator and its modifications are examined. The main features of the kiln are: length 80 m, outer diameter 2 m, rotational speed 0.75-0.95 rpm, inclination 3%, maximum output 135 tons per day of calcine (CaO·MgO), heavy fuel oil consumption 948.3 Lph at the maximum output [1]. The inclination and rotational speed enable counterflows of the exhaust gases and dolomite ($CaCO_3$·$MgCO_3$) inside the kiln [1].

The heat loss of the kiln shell was determined by the heat balance [1]. The loss was analytically verified in [1], by dividing the shell into 24 sections. The dissection was made according to the approximately equal surface temperatures. The total heat loss:

$$\dot{Q} = \sum_{i=1}^{24} \dot{Q}_{\mathrm{convs},i} + \sum_{i=1}^{24} \dot{Q}_{\mathrm{rad\,s},i} = \sum_{i=1}^{24} \alpha_{\mathrm{s},i} A_{\mathrm{s},i} \left(t_{\mathrm{s},i} - t_{\mathrm{o}}\right) + \sum_{i=1}^{24} \sigma \varepsilon A_{\mathrm{s},i} \left(T_{\mathrm{s},i}^4 - T_{\mathrm{o}}^4\right) \tag{1}$$

As the kiln is sheltered from the wind, the convective heat losses $\dot{Q}_{\mathrm{conv\,s},i}$ for all i sections were calculated by the model for free convection around a horizontal cylinder [19], taken from [20]. In each section i, the radiation heat loss $\dot{Q}_{\mathrm{rad\,s}}$ were calculated for the case of a pipe within a big room [21]. The model showed a good correlation with the energy balance [1] and was additionally used in the paper:

– in the case when enriched air is used for fuel combustion in the kiln to determine the heat loss based on the measured surface temperatures and
– to determine surface temperatures based on the known heat loss.

Table 1 shows heat losses from the kiln shell depending on the volume fraction of oxygen in the enriched air. The surface temperatures were measured [22], and used by eq. (1) to calculate the heat losses. The data are shown for the part of the kiln above the warmest zone

Table 1. The surface temperatures over the burning zone depending on the air enrichment; the first section is placed from 3.9-5.2 m from the burner's end of the kiln, *etc.*

O_2 [%]	Section, i	1	2	3	4	5	6	7
	Length, l_i	1.3	2	2.43	2.43	2.43	2.43	2.43
20.95	$t_{s,i}$ [°C]	328.0	319.0	332.0	364.0	304.0	263.0	229.0
	α [Wm^{-2}K^{-1}]	9.09	9.01	9.13	9.41	8.86	8.43	8.05
	Q [kW]	97.7	142.4	187.1	225.2	157.5	120.0	93.6
22	$t_{s,i}$ [°C]	332.2	324.1	336.8	371.1	307.9	267.2	232.1
	α [Wm^{-2}K^{-1}]	9.13	9.06	9.17	9.48	8.90	8.49	8.09
	Q [kW]	100.2	146.9	192.5	234.4	161.4	123.6	95.8
23	$t_{s,i}$ [°C]	337.3	329.8	341.7	378.1	313.2	272.2	236.8
	α [Wm^{-2}K^{-1}]	9.18	9.11	9.22	9.53	8.95	8.54	8.15
	Q [kW]	103.31	151.98	198.18	243.62	166.85	127.87	99.32

over which the recuperator should be placed. This area extends between 3.9 m and 19.35 m, see fig. 1. The first 3.9 m is a stationary part of the kiln that does not allow mounting the recuperator, whereas, after 19.35 m, the temperature decreases, and the kiln surface could be insulated [1].

Although the kiln operates in a steady-state, the surface temperatures always vary slightly, mainly because of many internal factors.

Modelling methods

An analytical cell modelling method is used to define the unknown geometry and operating parameters for the examined designs. In addition, a CFD model is used for validation and analyses of construction details, *i.e.*, as a sort of fine-tuning.

Cell modelling method

The recuperator is segmented into modelling cells according to the kiln surface temperatures. Depending on the design, each segment is modelled with two or three cells. Figure 3 shows these cells. Cells R_1 and R_2 describe the heat transfer in the recuperator and are based on the heat and mass rate balances. These cells are almost identical. The only difference is where the heat comes from: in R_1 from the kiln, and in R_2 from R_1. Cell I models the heat loss to the environment using heat rate balance.

The air that flows through the annular gap is heated by convective heat flow rates from the kiln, $\dot{Q}_{\mathrm{conv\,s},i}$, and the recuperator, $\dot{Q}_{\mathrm{rad\,s}}$, *i.e.*, in the i-th section:

$$\dot{Q}_{\mathrm{conv\,s},i} + \dot{Q}_{\mathrm{conv\,r},i} = \frac{\dot{m}_{\mathrm{a}}}{2} c_{p,\mathrm{a}} \left(t_{\mathrm{a,out},i} - t_{\mathrm{a,in},i} \right) \tag{2}$$

where $t_{\mathrm{a,in},i}$ and $t_{\mathrm{a,out},i}$ are the air inlet and outlet temperature in the section, respectively. For end sections $t_{a,\mathrm{in},1} = t_{\mathrm{a,in},8} = t_0$. Half of the mass-flow $\dot{m}_{\mathrm{a}}/2$ is used because two identical air streams flow towards the common extraction point, see fig. 1(a). Because of air and surface temperatures, see tab. 1, convection dominates the overall heat transfer. Therefore, a reliable determination of the heat transfer coefficients is of the highest importance as it determines the geometry of the annulus. The coefficients are the most significantly influenced by air velocity, whereas the air and surfaces temperatures, as well as the recuperator geometry, are influential factors too. To determine the convective heat flow rates, Position 1 in fig. 3, in eq. (2), heat transfer coefficients are calculated by the modified equation of Petukhov and Kirilov for fully developed turbulent flow in a concentric annular duct [23], as stated in [24]. The hydraulic diameter $d_{\mathrm{h},i}$ defined:

$$d_{\mathrm{h},i} = d_{\mathrm{r},i} - d \tag{3}$$

is the characteristic dimension be taken for the determination of heat transferred in the i^{th} section between the walls of the concentric annulus and the air that flows through it. To calculate the heat transfer coefficient in the i^{th} section, the physical properties are taken at the mean air temperature in the section.

The heat loss from the kiln shell in the i^{th} section $\dot{Q}_{\mathrm{s},i}$ is transferred by convection the air-flow or by thermal radiation the recuperator surface:

$$\dot{Q}_{\mathrm{s},i} = \dot{Q}_{\mathrm{conv\,s},i} + \dot{Q}_{\mathrm{rad\,sr},i} + \dot{Q}_{\mathrm{rad\,sr}(i-1),i} + \dot{Q}_{\mathrm{rad\,sr}(i+1),i} \tag{4}$$

The last three terms on the right-hand side of eq. (4) designate thermal radiation of the kiln surface towards the recuperator in the i^{th} section $\dot{Q}_{\mathrm{rad\,sr},i}$, and two adjacent sections: upstream $\dot{Q}_{\mathrm{rad\,sr}(i-1),i}$ and down stream $\dot{Q}_{\mathrm{rad\,sr}(i+1)}$. The radiation heat transfer rate between the surfaces of the kiln and the recuperator in the i^{th} section is [25]:

$$\dot{Q}_{\text{rad sr},i} = \frac{\sigma\left(T_{\text{s},i}^4 - T_{\text{r},i}^4\right)}{\left(\frac{1-\varepsilon_{\text{s}}}{\varepsilon_{\text{s}} A_{\text{s},i}}\right) + \frac{1}{F_{12} A_{\text{s},i}} + \left(\frac{1-\varepsilon_{\text{r}}}{\varepsilon_r A_{\text{r},i}}\right)} \tag{5}$$

where the view factor $F_{12} \approx 1$ is obtained by the graphical method [26]:

$$F_{12} = 1 - 2\tan^{-1}\frac{\left(\frac{d_{\text{r,i}} - d}{l_{\text{i}}}\right)}{\pi} \tag{6}$$

As $F_{12} \approx 1$, eq. (5) is similar to the equation for infinitely long concentric pipes.

The third, eqs. (2), (4), and (7), balance is the heat rate balance for the recuperator surface:

$$\dot{Q}_{\text{rad sr},i} + \dot{Q}_{\text{rad s}(i-1)\text{r},i} + \dot{Q}_{\text{rad s}(i+1)\text{r},i} = \dot{Q}_{\text{conv r},i} + \dot{Q}_{\text{r},i} \tag{7}$$

Three thermal radiation heat gains, left-hand side of eq. (7), are transferred by convection the air $\dot{Q}_{\text{conv r},i}$ and towards the second passage, see fig. 3(a), or the surroundings (see fig. 1 and 2), $\dot{Q}_{\text{r},i}$. When insulation thickness is known, $\dot{Q}_{\text{r},i}$ is calculated, otherwise, it is estimated. The convection term $\dot{Q}_{\text{conv r},i}$ in eq. (7) is calculated in the same manner as for the kiln surface. In eqs. (4) and (7), the terms that determine thermal radiation between the segment and the adjacent segments can be neglected because of:

– small view factors (less than 0.01) given

$$F_{i,(i-1)\text{or}(i+1)} = \tan^{-1}\frac{\left(\frac{d_{\text{r},i} - d}{l_{\text{i}}}\right)}{\pi} \tag{8}$$

– similar surface temperatures that almost cancel out radiation heat transfer rates between the adjacent sections, see tab. 1, and
– not fully opened the end sections towards the environment because of the use of radial blinds for air-flow control.

Through the validation of the model for the basic design, see fig. 1, in [1], the previous simplification was also validated.

The heat loss rate of the i^{th} section is transferred through a three-layer-cylindrical wall to the outer surface, from which the heat is transferred into the environment by convection and radiation:

$$\begin{aligned}\dot{Q}_{\text{r},i} &= \frac{T_{\text{r2},i} - T_0}{\frac{1}{2\pi\lambda_{\text{steel}}}\ln\frac{d_{\text{r3(2)},i}}{d_{\text{r2(1)},i}} + \frac{1}{2\pi\lambda_i}\ln\frac{d_{\text{i},i}}{d_{\text{r3(2)},i}} + \frac{1}{2\pi\lambda_{\text{Al}}}\ln\frac{d_{\text{io},i}}{d_{\text{i},i}}} = \\ &= \alpha_{\text{io},i} A_{\text{io},i}\left(t_{\text{io},i} - t_{\text{o}}\right) + \sigma\varepsilon_{\text{Al}} A_{\text{io},i}\left(T_{\text{io},i}^4 - T_{\text{o}}^4\right)\end{aligned} \tag{9}$$

The thermal conductivities for steel pipe λ_{steel}, mineral wool insulation λ_i, and aluminum sheet cover λ_{Al} are taken as in [27]. The heat transfer coefficient for natural-convection from the outer surface to the environment $\alpha_{\text{io},i}$ is taken from [20], and is identical to the heat loss from the bare kiln. The radiation from the outer surface is taken for the case of a pipe within a big room. The emissivity of the aluminum sheet ε_{Al} is taken from [21].

Recuperator with radiation fins

The RF recuperator, see figs. 2(b) and 3(b), is modeled similarly to RPP. Neglecting thermal radiation between the different sections as in eq. (7), the heat rate balances for the i^{th} section:

$$\dot{Q}_{\text{conv s},i} + \dot{Q}_{\text{conv r},i} + \dot{Q}_{\text{conv f},i} = \frac{\dot{m}_{\text{a}}}{2} c_{p,\text{a}} \left(t_{\text{a out},i} - t_{\text{a in},i} \right) \tag{10}$$

$$\dot{Q}_{\text{s},i} = \dot{Q}_{\text{conv s},i} + \dot{Q}_{\text{rad sr},i} + \dot{Q}_{\text{rad sf},i} \tag{11}$$

$$\dot{Q}_{\text{rad sf},i} = \dot{Q}_{\text{conv f},i} + \dot{Q}_{\text{rad fr},i} \tag{12}$$

$$\dot{Q}_{\text{rad sr},i} + \dot{Q}_{\text{rad fr},i} = \dot{Q}_{\text{conv r},i} + \dot{Q}_{\text{r},i} \tag{13}$$

These equations are heat rate balances: eq. (10) for the air-flow, eq. (11) for the kiln surface, eq. (12) for the fin, see fig. 3(b), and eq. (13) for the recuperator surface. The fin is connected to the recuperator. Compared with other surfaces involved in the heat transfer, the surface area of the connection is small. Because of that, its role in heat transfer is neglected.

The convective heat transfer rates in eqs. (10)-(13): at the kiln surface $\dot{Q}_{\text{conv s},i}$, at the surface of the recuperator $\dot{Q}_{\text{conv r},i}$, and at the fin $\dot{Q}_{\text{conv f},i}$ are calculated by the use of heat transfer coefficients that are calculated according to [24], cited by [23]. The Nusselt number eq. (14) is modified by taking into account the effect of temperature-dependent property variations, eq. (15). For the Prandtl number in the range $0.5 \leq \text{Pr} \leq 1.5$, these equations are:

$$\text{Nu}_{\text{m}} = 0.0214\left(\text{Re}^{0.8} - 100\right)\text{Pr}^{0.4}\left[1 + \left(\frac{d_{\text{h},i}}{l_i}\right)^{2/3}\right] \tag{14}$$

$$\text{Nu} = \text{Nu}_{\text{m}}\left(\frac{T_{\text{a,m},i}}{T_{\text{r},i}}\right)^{0.45} \tag{15}$$

The hydraulic diameter in eq. (14) is calculated by eq. (3). In eqs. (11)-(13) radiation heat transfer rates are calculated by an electric circuit analogy for heat exchange among diffuse gray bodies [23]:

$$\dot{Q}_{\text{rad sf},i} = \frac{\sigma\left(T_{\text{s},i}^4 - T_{\text{f},i}^4\right)}{\left(\frac{1-\varepsilon_s}{\varepsilon_{\text{s}} A_{\text{s},i}}\right) + \frac{1}{fA_{\text{s},i}} + \left(\frac{1-\varepsilon_{\text{f}}}{\varepsilon_{\text{f}} fA_{\text{f},i}}\right)} \tag{16}$$

$$\dot{Q}_{\text{rad sr},i} = \frac{\sigma\left(T_{\text{s},i}^4 - T_{\text{r},i}^4\right)}{\left(\frac{1-\varepsilon_{\text{s}}}{\varepsilon_{\text{s}} A_{\text{s},i}}\right) + \frac{1}{(1-f)A_{\text{s},i}} + \left(\frac{1-\varepsilon_{\text{r}}}{\varepsilon_{\text{r}} A_{\text{r},i}}\right)} \tag{17}$$

$$\dot{Q}_{\text{rad fr},i} = \frac{\sigma\left(T_{\text{f},i}^4 - T_{\text{r},i}^4\right)}{\left(\frac{1-\varepsilon_{\text{s}}}{\varepsilon_{\text{f}} fA_{\text{s},i}}\right) + \frac{1}{fA_{\text{f},i}} + \left(\frac{1-\varepsilon_{\text{r}}}{\varepsilon_{\text{r}} A_{\text{r},i}}\right)} \tag{18}$$

In eqs. (16)-(18), the view factors are determined by 2-D graphical method [24], and $f < 1$ is the relative closedness of the fin surface in the i-th segment:

$$f = 1 - \frac{A_{\mathrm{fo},i}}{A_{\mathrm{f},i}} \tag{19}$$

where $A_{\mathrm{fo},i}$ [m^2] is the total area of the openings on a radiation fin in the i^{th} section, and $A_{\mathrm{f},i}$ [m^2] is the total surface area of the radiation fin, see fig. 3(b). The purpose of the openings is to allow a part of radiation heat transfer to reach the recuperator surface. Figure 3(b) shows radiative heat transfer resistances for the examined recuperator.

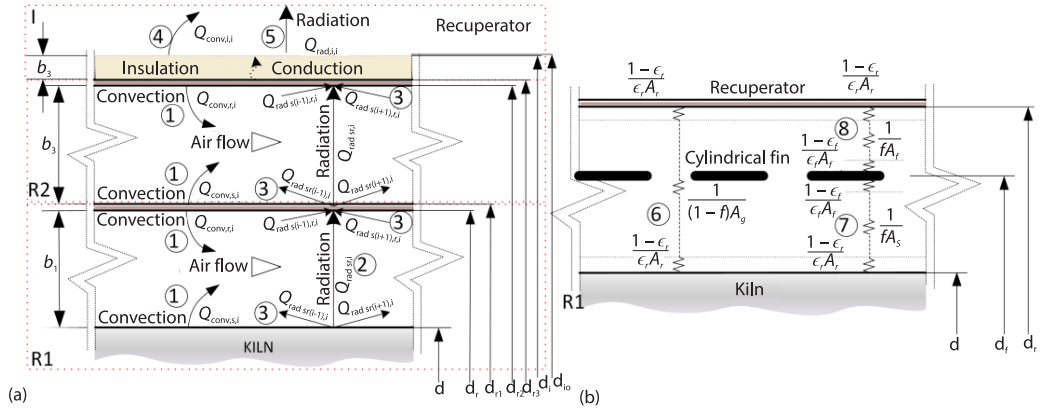

Figure 3. (a) Graphical illustration of the heat transfer and characteristic dimensions of the annular recuperator and (b) radiation heat transfer resistances and the schematic of the RF recuperator

In the presented models, the basic temperature-dependent thermodynamic properties for air (density, thermal conductivity, thermal diffusivity, dynamic viscosity, Prandtl number, specific heat capacity, and enthalpy) are calculated according to [28-30].

The CFD model

To simulate the experimental set-up and to indirectly validate the RF model as well as to examine the design details commercially available software ANSYS and its integration module FLUENT were used. In all simulations, the inlet/outlet pair: mass-flow inlet pressure outlet was used for the boundary condition. For compressible fluids, this is the most stable and the most frequently used pair of boundary conditions [31], defined by the mass-flow rate and temperature of the fluid at the inlet, and relative pressure of 0 Pa at the outlet. The applied model uses the energy equation, standard k-ε turbulent model, and the surface-to-surface radiation model. To solve the model, the pressure-velocity coupling method was used. It solved the model with the SIMPLEC scheme that used the heigh-order relaxation option. The absolute convergence criterion is that the residual for energy and all other quantities were less than $1 \cdot 10^{-5}$ and 0.001, respectively. The set convergence criteria were met before 500 iterations.

Validation of the RF model

Although it is composed of reliable heat transfer submodels, the RF model was experimentally validated. Figure 4 shows the experimental set-up, its picture, the average results, measuring errors, instruments, and methods. The connection between a wood pellet boiler and

a chimney is used for the experiment. Compared with the real conditions, the surface temperature in the experiment was lower and the innermost cylinder was not rotating. The velocity at the outer surface of the examined rotary kiln is lower than 0.14 m/s because of low rotational speed (below 0.95 rpm). Compared with the air velocities in the longitudinal direction, see tab. 3, 5, and 6, the velocity of the kiln is very low and its influence on the convective heat transfer can be neglected. Additionally, the comparison of CFD and cell models in the results section speaks in favor of the neglection. Although the surface temperature is lower, the temperature differences between the surfaces and between air and the surfaces are of the same magnitude as in real conditions.

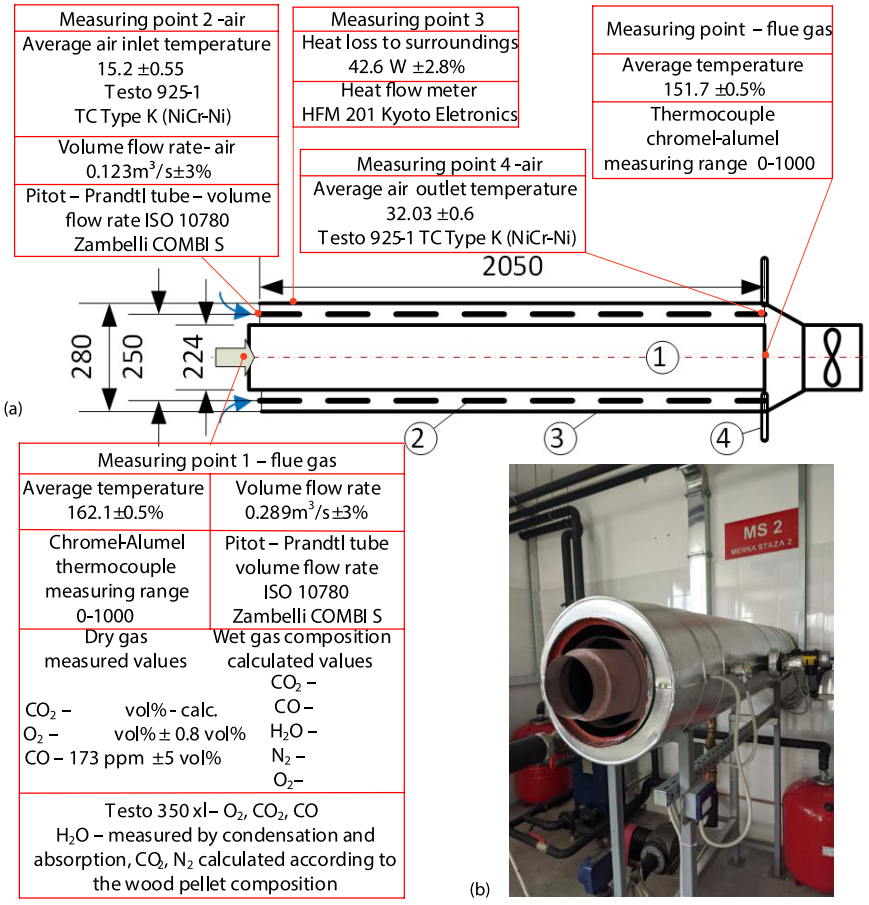

Figure 4. (a) Experimental set-up and measuring details: results, errors, instruments, and methods and (b) picture of the experimental set-up: *1 – flue gas pipe, 2 – radiation fin (f = 0.5, i.e., 50% of the radiation fins are hollow to enable radiative heat transfer from the kiln to the recuperator surface (see position – 2 and fig. 3 (b), 3 – recuperator, 4 – flow control dampers*

To compare the results of the experiment and the models, and to evaluate the accuracy of the experimental results, the uncertainty analysis is performed. The uncertainty R of a function F can be described as [32], cited by [13]:

$$W_R = \sqrt{\left(\frac{\partial F}{\partial x_1} W_{x_1}\right)^2 + \left(\frac{\partial F}{\partial x_2} W_{x_2}\right)^2 + \cdots + \left(\frac{\partial F}{\partial x_n} W_{x_n}\right)^2} \tag{20}$$

where x_1, x_2, …, x_n are independent variables and W_1, W_2, …, W_n are regarded as their corresponding uncertainties. The uncertainties are presented in tab. 2, except for the heat loss, which is given in fig. 4.

The RF cell could not be verified on its own by comparison with the experimental results. Because of that, the RF cell was combined with a flue gas cell, which was developed and validated in [27]. As this is a sort of indirect validation, the results are additionally checked with the simulation of the experimental set-up by the CFD model. For the CFD model, the mesh is composed of 1161.350 nodes and 1659.512 elements with the average quality of an element 0.301, and the average orthogonal quality of 0.7814. These parameters are used to evaluate the relative quality of the mesh. The quality is assessed by the number of elements and nodes that are quantitative indicators concerning: the volume and the shape in which the mesh is generated, the mesh density near the walls (borders) and at the cross-sections, the ratio between the height and length of an element, as well as the shape of an element.

In the CFD model, densities of air and flue gas are taken as for an ideal gas, whereas the specific heat capacity of the flue gas is calculated as for an ideal gas mixture. Figure 5 shows the simulation results for the CFD model depending on the position of the cross-section.

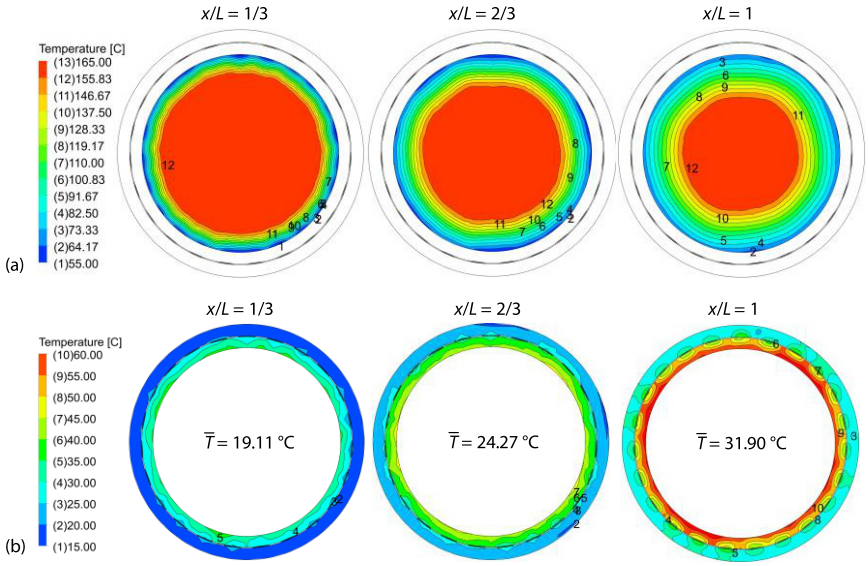

Figure 5. The simulation results of the CFD model for the experiment shown in fig. 4; (a) flue gas temperature and (b) air temperature; *x*/*L* represents the relative distance from the entry, see fig. 4

Table 2 shows the comparison between the experimental and the results of the developed and CFD model. The values show a good correlation, and the simulation results are within the measurement uncertainty.

Table 2. The uncertainties of the parameters obtained by the measuring results, see fig. 4, and comparison between the measured and values obtained from the cell and CFD models

Property	Area, A	ρ_{FG}	$\dot{m}_{FG}$	Δt_{FG}	$\dot{Q}_{FG}$	$\dot{m}_a$	Δt_a	Q_a
W	2.0%	5.1%	5.9%	10.7%	12.2%	3.6%	6.8%	7.5%
	Measurements		Model	CFD		Measurements	Model	CFD
$t_{a,\,out}$	32.03		32.13	31.90	Q [W]	2602	2556	2544
diff. [%]	–		0.3	0.4	diff. [%]	–	1.8	2.2

Results

The air preheated in the recuperator is extracted at the position placed so that both halves utilize equal heat losses of the kiln. The division enables the isothermal mixing of two air streams that leave the recuperator above the kiln section with the highest surface temperature, see fig. 1. Thermodynamically, this is advantageous because the temperature difference between the air and the kiln surface along the recuperator is analogous to that of counter-current heat exchangers, see tab. 1. Because of the division of the 4th section in tab. 1, there are 8 instead of 7 sections in the following analyses.

Figure 6(a) shows the air preheating temperatures depending on the minimal diameter, which is always at the air exit. Because all analyzed designs use the entire heat loss, the most efficient is the recuperator with the highest air exit temperature. With the rise of the minimum diameter for 5 cm, *i.e.*, if the annulus is increased by only 2.5 cm, the preheating temperature decreases by 107 °C. Smaller temperature differences between the air and the surfaces require larger heat transfer coefficients and consequently higher air velocities. Figure 6(a) shows the temperature differences between the air and the recuperator surface, whereas tab. 1 shows the temperature difference between the air and the kiln surface. The minimal diameter marginally influences the temperature of the recuperator. Figure 6(b) shows that the critical diameter can occur only if a high preheating temperature is a prime request.

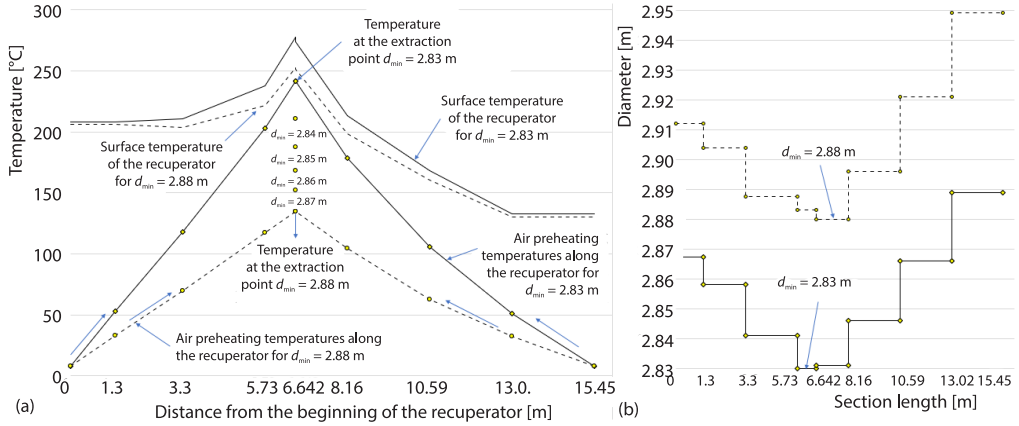

Figure 6. (a) The air and the temperatures of the recuperators along their lengths, and the maximal preheating temperatures depending on the minimal diameter and (b) the diameters along the recuperators with the minimal diameters of 2.83 and 2.88 m

For the smallest critical diameters of 2.83 and 2.84 m, the air velocities exceed only locally in the outlet sections recommended values for industrial ventilation [33]. Table 3 shows

the velocities for the design with the minimal diameter of 2.86 m. The table also shows the convective heat transfer rates from both surfaces to the air. The share of the recuperator surface in the total heat transfer rate to the air decreases with the decrease of the temperature difference between the air and the surfaces. As a result, the air outlet section should have a greater heat transfer area or air-flow. Table 3 shows the heat losses from the sections for a 5 cm thick mineral wool insulation.

Table 3. The design details for the recuperator with a minimum diameter of 2.86 m (the temperatures of the kiln shell are shown in tab. 1, these section lengths are used in the following tables)

Section, i	1	2	3	4′	4″	5	6	7
Length, l_i [m]	1.3	2	2.43	0.912	1.518	2.43	2.43	2.43
$t_{r,i}$ [°C]	206.7	206.7	225.6	258.5	256.6	202.1	162.7	131.0
$t_{a\,out,i}$ [°C]	38.6	83.0	141.2	167.3	167.3	123.8	74.8	37.3
$d_{h,i}$ [m]	0.094	0.086	0.069	0.06	0.06	0.076	0.099	0.125
w [m/s]	6.21	7.72	11.02	14.04	13.87	9.66	6.54	4.63
α [Wm^{-2}K^{-1}]	16.8	19.3	25.3	32.3	30.8	23.0	17.2	13.3
$\dot{Q}_{convs,i}$ [kW]	58.42	87.48	118.70	54.41	89.83	100.76	75.89	58.60
$\dot{Q}_{convr,i}$ [kW]	36.36	50.58	62.78	27.64	46.65	52.01	40.49	32.15
Q [kW[	1.63	2.49	3.41	1.54	2.53	2.93	2.22	1.69

Table 4 shows that for the equal minimal distances, the recuperator with the highest degree of emissivity has the largest air exit temperature. In this case, a higher degree of emissivity favors the thermal radiation from the kiln and hence the convection from the recuperator surface to the air.

Table 4. The influence of the degree of emissivity of the recuperator surface on the minimal diameter

	ε_s = 0.8 [1], ε_r = 0.97 [21] black paint			ε_s = 0.8 [1], ε_r = 0.8 oxidized surface			ε_s = 0.8 [1], ε_r = 0.144 [21] polished steel sheet		
d_{min} [m]	2.84	2.86	2.88	2.84	2.86	2.88	2.84	2.86	2.88
$\dot{m}_a/2$[kgs^{-1}]	2.41	3.08	3.75	2.465	3.16	3.89	3	4.13	5.4
t_p [°C]	211	167	139	205	163	134	171	127	99

Figure 7 illustrates the behavior of the recuperator under varying operating conditions of the rotary kiln. The surface temperatures that correspond to the heat losses are calculated by eq. (1) and the data are shown in tab. 1. Compared with the experimental results with enriched air shown in tab. 1, the variation of heat loss in a wider range is used. The design can be adapted to the varying operating conditions with the variation of the air-flow because of the similar temperature profiles, as can be seen in fig. 7(b). The recuperator cannot use the exact heat loss if the same air-flow is used for different operating conditions. Nevertheless, the deviation is negligible because of the previously mentioned surface temperature profile.

Figure 8 shows the simulation results for the recuperator with a minimum diameter of 2.83. The dimensions of the recuperator are shown in fig. 6(b) with a difference that a hood was added at the outlet to solve the problem of the head-on collision of two air streams. Without the hood, there would be turbulences, reversible flows, and a high pressure drop. The rotation of the kiln was included in the CFD model with a constant rotational velocity of 0.08901 rad/s.

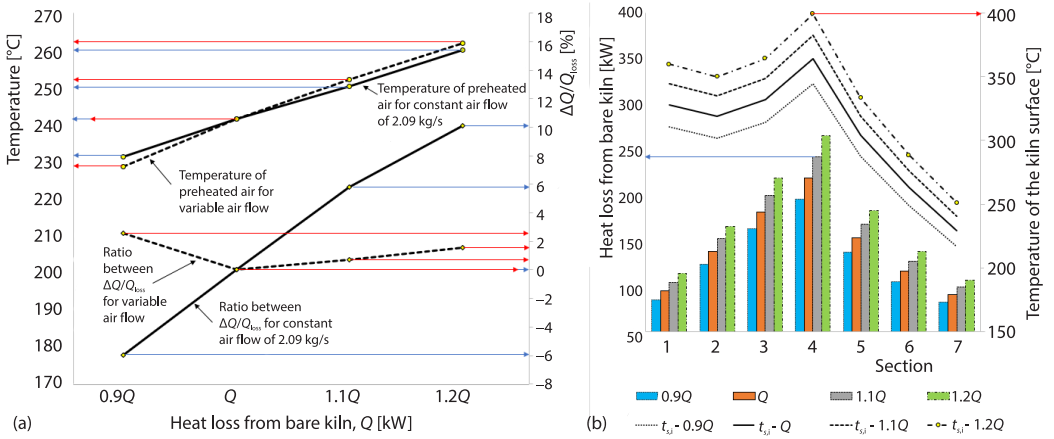

Figure 7. (a) The influence of the heat loss variation on the performance of the recuperator with the minimal diameter 2.83 m and (b) heat losses and corresponding surface temperatures (ΔQ is the difference between the examined and the nominal heat loss whereas Q_{loss} is the nominal heat loss)

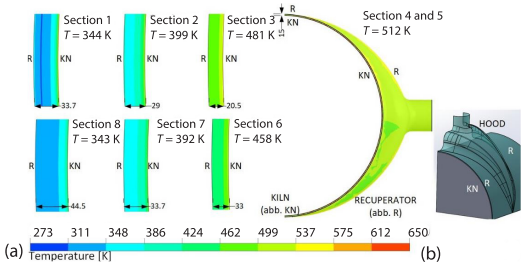

Figure 8. (a) The air temperature profiles at the exits of the sections for the recuperator with the minimal diameter of 2.83 m; the thicknesses of the annular gaps are given in mm and (b) 3-D drawing of the hood in the exit section

Because of the temperature symmetry, only a part of each cross-section and a half of the outlet section are shown. In the model, each section has a mesh that consists of 567.216 nodes and 544.787 elements, with the average quality of an element $1.583 \cdot 10^{-002}$ and the average orthogonal quality of 0.989. Because of a big difference in the dimensions of the air domain, the dimension of an element in the radial direction (20 elements in 30 mm with the growth coefficient of 1.2) is much smaller than in the longitudinal direction of 50 mm. It influences that the average quality of an element is not much higher than a minimum value of 0.01, which was recommended in [31]. The impact of the convective heat transfer at both surfaces is visible in fig. 8. Compared with the results shown in fig. 6(a), the difference between the temperatures at the exit is only 2 K. However, the biggest differences between the analytical and the CFD model are in the air inlet sections, 18 and 19 K.

The RPP design, which is shown in fig. 2(a), increases the surface area for convective heat transfer. Table 5 shows RPP dimensions and heat transfer details for the minimum inner diameter of 2.83 m. To support radiative heat transfer from the kiln surface, the degrees of emissivity for the recuperator surfaces are taken to be 0.97. To properly design RPP, an additional condition regarding the heat transfer is required. In the reported case, it was the minimal diameter of the inner passage of 2.83 m and the ratio of heat loss transferred to the air in the annuluses. After mixing all four streams, the air preheating temperature would be 210 °C. Compared with the basic design, figs. 1 and 5(a), for the same critical diameter, the preheating temperature for RPP is lower. The reason for this is the temperature of the kiln shell, which cannot transfer the

majority of the heat loss to the recuperator surface by thermal radiation. The positive features of the RPP design that allow very small gaps and usage of fins between the surfaces in the outer passage cannot be utilized except to prevent overheating of the outlet sections. The majority of the heat loss can be transferred to the surface of the recuperator and the second annulus only at the air exit sections because there, thermal radiation from the kiln surface is accompanied with the cooling of already preheated air. The isothermal mixing of four streams is possible and is achievable only when a small fraction of air-flows through the outer passage, *e.g.*, for the minimum diameter in the inner annulus of 2.88 m, isothermal mixing at 138 °C is achieved if two air streams of 6.926 kg/s and 0.606 kg flow through the inner and outer annuluses, respectively.

Table 5. The geometry and heat transfer details for RPP with a minimum inner diameter of 2.83 m; mass-flow rates: in the inner 1.616 kg/s, and the outer annulus 0.8051 kg/s, (ε = 0.8, ε_r= 0.97)

Section, i	1	2	3	4′	4″	5	6	7
$t_{r,i(R1)}$ [°C]	181.9	184.6	200.9	233.4	244.0	178.7	146.7	112.7
$t_{a\,out,i(R1)}$ [°C]	55.0	121.9	198.9	233.2	233.3	175.1	109.9	53.2
d_r [m]	2.863	2.854	2.84	2.831	2.831	2.844	2.86	2.881
$w_{(R1)}$ [ms–1]	5.05	7.00	11.36	16.36	16.33	9.89	6.17	3.90
$\alpha_{(R1)}$ [Wm^{-2}K^{-1}]	14.87	18.88	27.93	39.04	38.48	25.29	17.45	12.18
$Q_{conv\,s,i(R1)}$ [kW]	50.39	76.55	102.40	50.93	77.13	87.27	67.64	51.61
$Q_{conv\,r,i(R1)}$ [kW]	26.22	32.67	24.59	6.05	19.48	19.93	24.89	22.05
$t_{r,i(R2)}$ [°C]	118.3	124.9	138.7	163.4	181.5	120.3	96.8	65.8
$t_{a\,out,i(R2)}$ [°C]	30.6	66.3	133.3	163.3	163.3	115.0	58.8	29.3
d_{r2} [m]	2.98	2.948	2.886	2.860	2.881	2.893	2.962	3.008
$w_{(R2)}$ [ms^{-1}]	1.37	1.94	5.30	11.51	5.32	4.77	1.74	1.24
$\alpha_{(R2)}$ [Wm^{-2}K^{-1}]	5.79	7.41	17.84	36.33	17.12	16.64	6.90	5.39
$Q_{conv\,s,i(R2)}$ [kW]	11.04	18.15	39.21	27.66	22.85	33.26	15.52	11.18
$Q_{conv\,r,i(R2)}$ [kW]	6.97	10.49	15.27	4.93	9.35	12.28	8.23	5.83

Unlike the RPP design, the introduction of radiation fins, see fig. 2(b), has a positive effect on the critical diameter. Compared with the basic design with the minimal diameter of 2.84 m, see fig. 5(a), RF, see fig. 2(b), and tab. 6, with the fins at the diameter of 2.84 m has more than 30 °C higher preheating temperature. A larger surface area for the convective heat transfer causes the improvement. Compared with the basic design, the surface area is more than 60% larger, but the benefit is modest because the majority of the heat loss is transferred to the air by convection at the kiln surface. The kiln shell temperature limits the impact of thermal radiation. It decreases with the rise of air temperature. Table 6 shows that the distance between the radiation fin and the recuperator becomes very small near the exit. That suggests that instead of the use of radiation fins, the recuperator surface should be finned in the outlet sections. In fact, in the air outlet sections preferable option is the application of fins on the kiln surface.

Table 6. The geometry and heat transfer details of the RF design with radiation fins at 2.84 m; mass-flow rate is 3.52 kg/s ($\varepsilon_s = 0.8$, $\varepsilon_{f,i} = 0.97$, $\varepsilon_r = 0.97$)

Section, i	1	2	3	4′	4″	5	6	7
$t_{fr,i}$ [°C]	177.8	189.5	230.4	263.1	257.4	206.9	152.8	112.3
$t_{r,i}$ [°C]	163.4	178.8	221.5	253.2	246.3	200.5	144.4	102.2
$t_{a\,out,i}$ [°C]	61.5	139.0	239.6	243.3	243.3	209.6	124.6	59.3
d_r [m]	2.89	2.87	2.842	2.844	2.847	2.847	2.876	2.909
d_f [m]	2.84	2.84	2.84	2.84	2.84	2.84	2.84	2.84
f	0.60	0.60	0.66	0.70	0.70	0.60	0.60	0.60
w [ms^{-1}]	4.05	6.36	13.90	18.20	16.67	11.70	5.74	3.27
α [Wm^{-2}K^{-1}]	13.80	19.20	36.80	46.70	41.85	32.60	18.20	11.70
$Q_{conv\,s,i}$ [kW]	46.31	74.05	112.41	51.80	83.79	95.40	66.57	48.92
$Q_{conv\,f,i}$ [kW]	27.51	36.77	43.33	19.86	34.37	33.72	28.85	24.00
$Q_{conv\,r,i}$ [kW]	20.96	27.25	25.74	10.39	18.32	23.65	20.96	17.84

Conclusions

Regarding the defined goals, the main conclusions are as follows.

- For a given minimal diameter defined by the rotational eccentricity of the kiln, a maximum air preheating temperature exists. The eccentricity is the most influencing parameter that defines the efficiency of the recuperator for the given heat loss and surface temperatures.
- The annular recuperator can be applied under variable operating conditions of rotary kilns (*e.g.*, combustion with enriched air) if there is no significant change in the surface temperature profile.
- The distance between the surfaces of the kiln and the recuperator can be increased by the use of higher degrees of emission, fins, and an additional air-flow in the critical sections. The usage of the design with the second annulus (RPP) should be avoided. It could be applied only over the air outlet section prevent the overheating of the kiln surface.
- In the analyzed designs, the air velocity does not exceed the recommended values.
- The introduction of additional air-flow should be considered only for the air outlet section and in the combination of two basic designs. The latter is recommendable for rotary kilns that have tyres over their hottest zones.
- The use of radiation fins has a modest effect on the efficiency of the recuperator, as convection at the kiln surface dominates the overall heat transfer. There is a need for this kind of fins only in the outlet section.
- The use of different designs or collapsible longitudinal fins in the outlet section enables the utilization of all available heat and decreases the distance between the kiln and the recuperator. The modifications of the design should be as simple as possible and should enable: mixing of two air streams, the precise use of the available heat, and a low pressure drop.

Acknowledgment

This research was supported by the Ministry of Education, Science and Technological Development of the Republic of Serbia (Grant No. 451-03-9/2021-14/200108).

Nomenclature

A – surface area, [m^2]
$A_{fo,i}$ – the total area of the openings on a radiation fin in the i^{th} section, [m^2]
$A_{f,i}$ – the total surface area of the radiation fin in the i^{th} section, [m^2]
$c_{p,a}$ – specific heat capacity of air at constant pressure, [kJkg^{-1}K^{-1}]
d – external diameter of the kiln, 2.8 m
d_h – hydraulic diameter, [m]
d_{min} – minimal (critical) diameter of the recuperator, [m]
d_r, d_{r1}, d_{r2}, d_{r3}, $d_{i,i}$, $d_{io,i}$ – diameters defined in fig. 3, [m]
F_{12} – view factor, [–]
f – relative closedness of the fin, [–]
l – length, [m]
$\dot{m}$ – mass-flow rate, [kgs^{-1}]
Nu – Nusselt number, [–]
Pr – Prandtl number, [–]
Q – heat loss, [kW]
$\dot{Q}$ – heat flow rate, [kW]
$\dot{Q}_{rad}$ – radiative heat flow rate, [kW]
Re – Reynolds number, [–]
R_1, R_2 – cells, see fig. 3.(a)
t – temperature, [°C]
T – temperature, [K]
w – air velocity, [ms^{-1}]
W_1,..., W_n – uncertainties, [–]
x_1,., x_n – independent variables, [–]

Greek letters

α – convective heat transfer coefficient, [Wm^{-2}K^{-1}]
ε – emissivity, [–]
λ – thermal conductivity, [Wm^{-1}K^{-1}],
σ – Steffan-Boltzmann coefficient, 5.67·10^{-8} [Wm^{-2}K^{-4}]
ρ – density, [kgm^{-3}]

Subscripts

a – air
Al – aluminum
conv – convection
FG – flue gas
f – fin
i – ith section or insulation
i,i – in the ith section of the recuperator
(i–1) – in the upstream cell
(i+1) – in the downstream cell
i+1 – upstream section,
i-1 – downstream section,
in – designates quantity that enters,
io – the outer surface of the insulation,
m – modified
,m – mean,
o – ambient or outer
out – designates all streams leaving the kiln, or air leaving the i^{th} section of the recuperator
p – preheating
r – recuperator
rad – radiation
s – designates the outer surface of the kiln
s,i – ith section of the kiln outer surface
sr, sf, fr – designate radiative heat transfer between any of two surfaces of: the klin (s), the recuperator (r), and the fin (f)
steel – steel
1 or R1 – inner segment in the RPP design
2 or R2 – outer segment in the RPP design

References

[1] Karamarković, V., *et al*., Recuperator for Waste Heat Recovery from Rotary Kilns, *Appl. Therm. Eng*., *54* (2013), 2, pp. 470-480
[2] Vijayan, S. N., Sendhilkumar, S., Industrial Applications of Rotary Kiln in Various Sectors – A Review, *Int. J. Eng. Innov. Res*., *3* (2014), Jan., pp. 342-345
[3] Golewski, G. L., Energy Savings Associated with the Use of Fly Ash and Nanoadditives in the Cement Composition, *Energies*, *13* (2020), 9, 2184
[4] ***, U. S. G. Survey, National Minerals Information Center, (n.d.). https://www.usgs.gov/centers/nmic/mineral-commodity-summaries
[5] Caputo, A. C., *et al.*, Performance Modelling of Radiant Heat Recovery Exchangers for Rotary Kilns, *Appl. Therm. Eng*., *31* (2011), 14-15, pp. 2578-2589
[6] Chakrabati, B., Investigations on Heat Loss through the Kilne Shell in Magnesite Dead Burning Process: A Case Study, *Appl. Therm. Eng*., *22* (2002), 12, pp. 1339-1345
[7] Sadighi Sepehr, A. A., Mansoor, S., Rotary Cement Kiln Coating Estimator: Integrated Modelling of Kiln with Shell Temperature Measurement, *Can. Jouranl Chem. Eng*., *89* (2011), 1, pp. 116-125
[8] Engin, T., Ari, V., Energy Auditing and Recovery for Dry Type Cement Rotary Kiln Systems – A Case Study, *Energy Convers. Manag*., *46* (2005), 4, pp. 551-562
[9] Kabir, G., *et al*., Energy Audit and Conservation Opportunities for Pyroprocessing Unit of a Typical Dry Process Cement Plant, *Energy*, *35* (2010), 3, pp. 1237-1243

[10] Luo, Q., *et al*., A Thermoelectric Waste-Heat-Recovery System for Portland Cement Rotary Kilns, *Journal Electron. Mater*., *44* (2015), Dec., pp. 1750-1762
[11] Mirhosseini, M., *et al*., Power Optimization and Economic Evaluation of Thermoelectric Waste Heat Recovery System around a Rotary Cement Kiln, *Journal Clean. Prod*., *232* (2019), Sept., pp. 1321-1334
[12] Mittal, A., Rakshit, D., Energy Audit and Waste Heat Recovery from Kiln Hot Shell Surface of a Cement Plant, *Therm. Sci. Eng. Prog*., *19* (2020), 100599
[13] Du, W. J., *et al*., Experiments on Novel Heat Recovery Systems on Rotary Kilns, *Appl. Therm. Eng*., *139* (2018), Apr., pp. 535-541
[14] Yin, Q., *et al*., Optimization Design and Economic Analyses of Heat Recovery Exchangers on Rotary Kilns, *Appl. Energy*., *180* (2016), Oct., pp. 743-756
[15] Yin, Q., *et al*., Design Requirements and Performance Optimization of Waste Heat Recovery Systems for Rotary Kilns, *Int. J. Heat Mass Transf*., *93* (2016), Feb., pp. 1-8
[16] Akram, N., *et al*., Improved Waste Heat Recovery through Surface of Kiln Using Phase Change Material, *Thermal Science*, *22* (2018), 2, pp. 1089-1098
[17] Zheng, K., *et al*., Rotary Kiln Cylinder Deformation Measurement and Feature Extraction Based on EMD Method, *Eng. Lett*., *23* (2015), 4, pp. 283-291
[18] Mirzakhani, M. A., *et al*., Energy Benchmarking of Cement Industry, Based on Process Integration Concepts, *Energy*., *130* (2017), July, pp. 382-391
[19] Churchill. W. C. H., Correlating Equations for Laminar and Turbulent Free Convection from a Horizontal Cylinder, *Int. J. Heat Mass Transf*., *18* (1975), 9, pp. 1049-1053
[20] Werner Kast, H. K., *Heat Transfer by Free Convection: External Flows, in: VDI Heat Atlas*, 2nd ed., Springer, Heidelberg, Germany, 2010, pp. 667-672
[21] Kabelac, D., Vortmeyer, S., Radiation of Surfaces, in: *VDI Heat Atlas*, Heidelberg, Germany, 2010, pp. 947-959
[22] Karamarkovic, V., *et a*l., The Impact of the Usage of enriched Air for Combustion on the Kiln Production, (in Serbian), Report No. 01-11/2012-MF-CTTZZS, Mechanical Faculty in Kraljevo, Kraljevo, Serbia, 2012
[23] Gnielinski, V., Forced Convection, in: *VDI Heat Atlas*, 2nd ed., Heidelberg, Germany, 2010, pp. 691-699
[24] Gnielinski, V., New Equations for Heat and Mass Transfer in Turbulent Pipe and Channel Flow, *Int. J. Chem. Eng*., *16* (1976), 3-4, pp. 359-368
[25] Janna, S. W., *Engineering Heat Transfer*, 3rd ed., CRC Press, Boka Raton, Fla., USA, 2009
[26] Vormeyer, D., Kabelac, S., View Factors, in: *VDI Heat Atlas,* Heidelberg, Germany, 2010, pp. 961-978
[27] Knežević, D. S., *et al.*, Radiant Recuperator Modelling and Design, *Thermal Science*, *21* (2017), 2, pp. 1119-1134
[28] Kleiber, M., Joh, R., Calculation Methods for Thermopysical Properties, in: *VDI Heat Atlas*, 2nd ed., Springer, Heidelberg, Germany, 2010, pp. 121-152
[29] Kleiber, M., Joh, R., Properties of Selected Importanat Pure Substances, in: *VDI Heat Atlas*, 2nd ed., Heidelberg, Germany, 2010, pp. 153-299
[30] Kleiber, M., Joh, R., Properties of Pure Fluid Substances, in: *VDI Heat Atlas*, 2nd ed., Heidelberg, Germany, 2010, pp. 301-417
[31] Sofialidis, D., Boundary Conditions AND Solver Settings, https://events.prace-ri.eu/event/156/contributions/6/attachments/65/89/Fluent-Intro_14.5_L02_BoundaryConditionsSolverSettings.pdf, 2013, p. 61
[32] Moffat, R. J., Describing the Uncertainties in Experimental Results, *Exp. Therm. Fluid Sci*., *1* (1988), 1, pp. 3-17
[33] ***, e-ToolBox, Velocity Classification of Ventilation Ducts, https://www.engineeringtoolbox.com/velocities-ventilation-ducts-d_211.html, 2013

Paper submitted: April 10, 2021
Paper revised: July 12, 2021
Paper accepted: July 14, 2021